Tubular Adhesive Joints Under Axial Load

N. Pugno
e-mail: nicola.pugno@polito.it

A. Carpinteri
e-mail: alberto.carpinteri@polito.it

Department of Structural Engineering,
Politecnico di Torino,
Corso Duca Degli Abruzzi 24
10129 Torino, Italy

In this paper a general study on tubular adhesive joint under axial load is presented. We focus our attention on both static and dynamic behavior of the joint, including shear and normal stresses and strains in the adhesive layer, joint optimization, failure load for brittle crack propagation, and crack detection based on free vibrations. First, we have considered the shear and normal stresses and strains in the adhesive layer to propose an optimization to uniform axial strength (UAS) and to reduce the stress peaks in the bond. The stress analysis confirms that the maximum shear stresses are attained at the ends of the adhesive and that the peak of maximum shear stress is reached at the end of the stiffer tube and does not tend to zero as the adhesive length approaches infinity. A fracture energy criterion to predict brittle crack propagation for conventional and optimized joint is presented. The stability of brittle crack propagation and the strength of the joint, as well as the ductile-brittle failure transition, are analyzed. A detection method to predict crack severity, based on joint dynamic behavior, is also proposed. The crack detection is achieved through the determination of the axial natural frequencies of the joint as a function of the crack length, by determining the roots of a determinantal equation.
[DOI: 10.1115/1.1604835]

1 Introduction

Based on modern synthetic adhesives, light, stiff, and economic constructions can be fabricated from a variety of materials without the defects caused by conventional assembly methods, such as welding, soldering, and riveting. Furthermore, together with mechanical strength and stiffness, a number of extra benefits come along free, like sealing action, electrical and thermal insulation, corrosion, and fretting resistance. As a consequence, various kinds of adhesive-bonded joints have been used in the manufacturing of light structures. For example, an analysis was carried out on bonded airframe components from an original Comet aircraft, which was over 30 years old. Redux phenolic adhesives were used extensively to bond stringer/panel assemblies. By careful removal of the bonded areas from the stiffener flange/panel it was possible to obtain lap and wedge cleavage test pieces. The same generic adhesive product continues to be used in current airframe construction. It can be seen that strength and durability of the old Comet test pieces are only about 10% lower than new joints, and some of the differences may be attributable to improvements in the new adhesive rather than degradation of the old joints, [1].

Since the pioneering papers by Goland and Reissner [2], Lubkin and Reissner [3], and more recently by Adams and Peppiatt [4], Renton and Vinson [5], Delale and Erdogan [6], and Chen and Cheng [7], several theoretical, numerical, and experimental analysis on tubular bonded joints have been performed. Only recently nontubular structures have been investigated by Pugno et al. [8–10].

In this paper we propose a special type of tubular joint with tapered adherends, produced by modifying the joint profile and thereby optimizing the tubular joint for uniform axial strength (UAS). As a consequence, the predominant component of the adhesive stress tensor (equivalent to the applied axial load) becomes constant, and the stress peaks of the other components are drastically reduced. This result is of considerable practical utility and makes it possible to produce adhesive bonded joints which are both lighter and stronger under axial load. An analogous optimization for uniform torsional strength (UTS) has been presented in [11].

The brittle failure load for a tubular adhesive joint under axial load, as well as a dynamical approach to crack detection are investigated. A very general formula has been obtained by means of the Griffith [12] energy balance and the application of linear elastic fracture mechanics (see Carpinteri's papers [13–17,18]). It is supposed that crack propagation at the interface between the two adherends takes place in mode I in the adhesive at the point of highest stress concentration, deduced by stress analysis. An energy balance is formulated for a small growth of the debonding: Changes in the strain energy of the joint and in the potential energy of the loading device are equated to the characteristic energy needed for debonding, [19,20]. As a consequence, a general formula to predict the brittle failure load for a tubular adhesive joint with or without UAS tapered adherends can be obtained. This formula generalizes an analogous formula already presented in the literature for tubular joint between a perfectly rigid and an elastic nontapered tubes, [19]. The greater sensitivity to brittle collapse is emphasized for the conventional geometry, if it is compared with the UAS optimized profile one. The stability of brittle crack propagation and the size effects on mechanical collapse behavior, as well as the ductile-brittle transition are emphasized.

A detection method to predict the crack length, influencing the strength of the joint, based on the joint dynamic behavior, is also presented. The study of the joint dynamics provides a system of coupled differential equations with partial derivatives. The crack detection is achieved through the determination of the axial natural frequencies of the damaged joint as a function of the crack length, by determining the roots of the corresponding determinantal equation. This approach has already been successfully applied to the study of undamaged bonded joints under torsion, [21].

Relevant general works on bonded joints and composite materials can be founded in [22–28].

2 Shear Stresses

It is assumed that all three of the materials making up the joint (tubes and adhesive) are governed by isotropic linear elasticity. The tubular bonded joint, consisting of two tubes perfectly circular and co-axial and the interposed adhesive's film (of very small

Contributed by the Applied Mechanics Division of THE AMERICAN SOCIETY OF MECHANICAL ENGINEERS for publication in the ASME JOURNAL OF APPLIED MECHANICS. Manuscript received by the ASME Applied Mechanics Division, June 5, 2002; final revision, Feb. 12, 2003. Associate Editor: M.-J. Pindera. Discussion on the paper should be addressed to the Editor, Prof. Robert M. McMeeking, Department of Mechanical and Environmental Engineering, University of California–Santa Barbara, Santa Barbara, CA 93106-5070, and will be accepted until four months after final publication of the paper itself in the ASME JOURNAL OF APPLIED MECHANICS.

 Copyright © 2003 by ASME

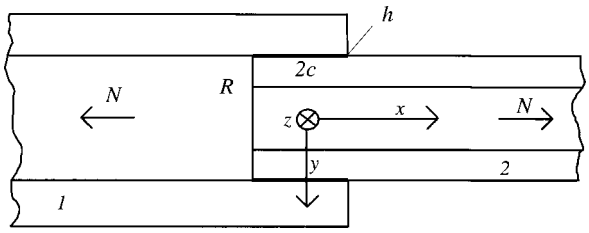

Fig. 1 Tubular adhesive joint subjected to axial load

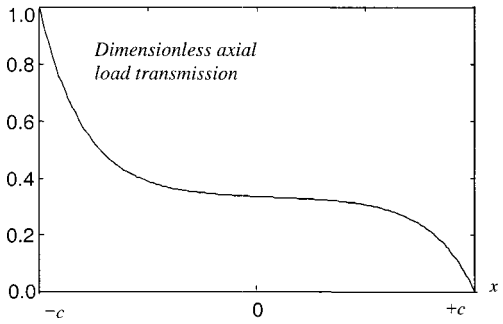

Fig. 2 Qualitative diagram (α=1, β=1/3) for dimensionless axial load transmission $f(x)$

thickness h, axial length $2c$, and radius R), is considered to be subject to axial load (Fig. 1). Under these conditions, the axial equilibrium along the x-axis permits to obtain the predominant component of adhesive stress tensor, equivalent to the applied normal thrust:

$$\tau_{rx}(x) = -\frac{1}{2\pi R}\frac{\mathrm{d}N_1(x)}{\mathrm{d}x}, \tag{1}$$

where $N_1(x)$ is the axial load of the outer tube in a generic x section. As a consequence of the axial symmetry, the other components of the stress tangential field can be neglected:

$$\tau_{r\vartheta}(x) \approx 0, \quad \tau_{x\vartheta}(x) \approx 0. \tag{2}$$

The strain component γ_{rx} in the adhesive can be obtained as

$$\gamma_{rx}(x) = \frac{\tau_{rx}(x)}{G_a} = -\frac{1}{2\pi R G_a}\frac{\mathrm{d}N_1(x)}{\mathrm{d}x}, \tag{3}$$

where G_a is the shear elastic modulus of the adhesive. Obviously we have

$$\gamma_{r\vartheta}(x) \approx 0, \quad \gamma_{x\vartheta}(x) \approx 0. \tag{4}$$

The axial load $N_i(x)$ in a generic section x of the tube i can be written as

$$N_1(x) = Nf(x), \quad N_2(x) = N(1-f(x)), \tag{5}$$

as the sum of the forces absorbed by the two elements must be equivalent to the applied axial load N at each cross section x. Satisfying the load boundary conditions implies

$$f(x=-c) = 1, \quad f(x=+c) = 0. \tag{6}$$

Function $f(x)$, and thus the load absorbed by the two elements at the joint, can be found thanks to the compatibility established for the displacements of the two tubes in a given cross sections. These displacements are expressed as follows:

$$u_1(x) = \int_{-c}^{x} \frac{N_1(t)}{E_1 A_1}\mathrm{d}t + u_1^0, \tag{7a}$$

$$u_2(x) = \int_{-c}^{x} \frac{N_2(t)}{E_2 A_2}\mathrm{d}t + u_2^0, \tag{7b}$$

where E_i is the Young's modulus, A_i is the cross-section area, and u_i^0 is the displacement of the initial section ($x=-c$), of the tube i. Through an appropriate choice of reference system, we can always have $u_1^0 = 0$ (displacements calculated starting from the strained configuration of the first tube's initial section).

The compatibility equation can be written noting how, after the joint deformation, the relative displacement Δu between two points of interfaces, internal tube-adhesive, and adhesive-external tube, must be the same if we consider the tubes' relative displacement or the shearing adhesive's strain (with a very small thickness h):

$$\Delta u = u_2 - u_1 = h\gamma_{rx}(x). \tag{8}$$

Substituting Eq. (3) into Eq. (8), the compatibility equation can be rewritten as

$$\frac{\mathrm{d}N_1(x)}{\mathrm{d}x} = -K^*\Delta u(x), \quad K^* = \frac{2\pi R G_a}{h}, \tag{9}$$

where K^* is the adhesive stiffness per unit length.

Inserting the displacement expressions (7) in the compatibility Eq. (9), and recalling Eqs. (5) and (6), gives the following second-order differential equation in $f(x)$:

$$\frac{\mathrm{d}^2 f(x)}{\mathrm{d}x^2} - \frac{K^*(E_1A_1+E_2A_2)}{E_1A_1E_2A_2}f(x) = -\frac{K^*}{E_2A_2},$$

$$\text{boundary conditions } \begin{cases} f(x=-c)=1 \\ f(x=c)=0 \end{cases}. \tag{10}$$

This differential equation, together with the boundary conditions shown alongside, makes it possible to determine the load section by section at the overlap. The solution of Eq. (10) is

$$f(x) = C_1 e^{\alpha x} + C_2 e^{-\alpha x} + \beta, \quad \alpha = \sqrt{\frac{K^*(E_1A_1+E_2A_2)}{E_1A_1E_2A_2}},$$

$$\beta = \frac{E_1A_1}{E_1A_1+E_2A_2}. \tag{11}$$

The constants C_1 and C_2 can be obtained from the boundary conditions as

$$C_1 = \frac{e^{-\alpha c}}{e^{-2\alpha c}-e^{2\alpha c}} + \beta\frac{e^{\alpha c}-e^{-\alpha c}}{e^{-2\alpha c}-e^{2\alpha c}}, \tag{12a}$$

$$C_2 = \frac{e^{\alpha c}}{e^{2\alpha c}-e^{-2\alpha c}} + \beta\frac{e^{-\alpha c}-e^{\alpha c}}{e^{2\alpha c}-e^{-2\alpha c}}. \tag{12b}$$

Comparing the differences between Eqs. (7) with the same obtained by Eq. (9), makes it possible to determine the constant u_2^0, once the reference system has been established with $u_1^0 = 0$:

$$u_2^0 = \frac{N\alpha}{K^*}(C_2 e^{\alpha c} - C_1 e^{-\alpha c}). \tag{13}$$

Function $f(x)$, being known (see Eqs. (11), (12), and Fig. 2), finally we can obtain the predominant shear stress in the adhesive:

$$\tau_{rx}(x) = -\frac{N}{2\pi R}\frac{\mathrm{d}f(x)}{\mathrm{d}x}. \tag{14}$$

The maximum shear stresses are reached at the ends of the adhesive and the higher stress peak appears at the end of the stiffer tube. When the stiffnesses of the two tubes are equal (β=1/2), the stress peaks become lower and symmetric (Fig. 3). The presented stress approach has already been validated numerically for the case of nontubular bonded joints. The discrepancy on stress peak appears lower than 5%, [10].

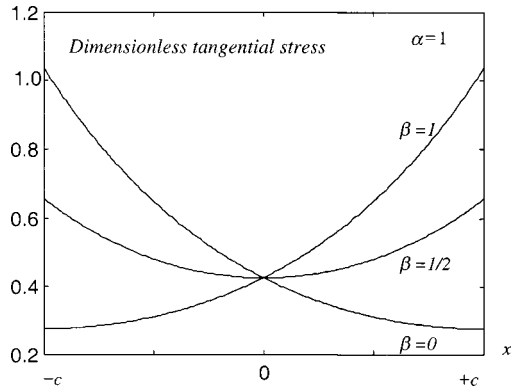

Fig. 3 Qualitative diagram for the dimensionless tangential stress $-df(x)/dx$

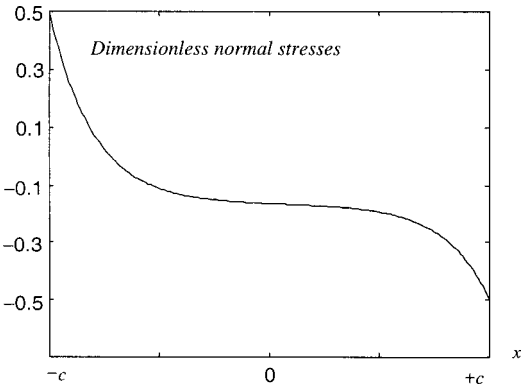

Fig. 4 Qualitative diagram (α=1, β=1/3) for the dimensionless normal stresses ($f(x)-1/2$)

This analysis does not include transverse shear deformation and because of this maximum shear stresses occur very near to but not at the ends of the joints. Obviously, the shearing stresses must be zero at the ends of the joint because there can be no shear stresses on the adhesive free surface, hence no shear stresses in the adhesive at the joint end because of equilibrium. For more details on transverse shear deformation see [22].

3 Normal Stresses

If $v_i(r,x)=-\nu_i N_i/(E_iA_i)r$ is the radial displacement of the tube i (ν_i is its Poisson's ratio), we can obtain the dilations imposed to the adhesive layer ($r\cong R$):

$$\varepsilon_r(x)=\frac{v_1(R,x)-v_2(R,x)}{h}=\frac{NR}{h}\left(\frac{\nu_2(1-f(x))}{E_2A_2}-\frac{\nu_1 f(x)}{E_1A_1}\right), \tag{15a}$$

$$\varepsilon_\theta(x)=\frac{\Delta R}{R}=\frac{v_1(R,x)+v_2(R,x)}{2R}=\frac{N}{2}\left(\frac{\nu_2(f(x)-1)}{E_2A_2}-\frac{\nu_1 f(x)}{E_1A_1}\right), \tag{15b}$$

$$\varepsilon_x(x)=\frac{\partial(u_1(x)+u_2(x))}{2\,\partial x}=\frac{N}{2}\left(\frac{f(x)}{E_1A_1}+\frac{(1-f(x))}{E_2A_2}\right), \tag{15c}$$

and the normal stresses by the constitutive equations for the adhesive,[18],

$$\sigma_x(x)=\frac{(1-\nu_a)E_a}{(1+\nu_a)(1-2\nu_a)}\varepsilon_x(x)+\frac{\nu_a E_a}{(1+\nu_a)(1-2\nu_a)}(\varepsilon_r(x)+\varepsilon_\theta(x)), \tag{16a}$$

$$\sigma_r(x)=\frac{(1-\nu_a)E_a}{(1+\nu_a)(1-2\nu_a)}\varepsilon_r(x)+\frac{\nu_a E_a}{(1+\nu_a)(1-2\nu_a)}(\varepsilon_x(x)+\varepsilon_\theta(x)), \tag{16b}$$

$$\sigma_\theta(x)=\frac{(1-\nu_a)E_a}{(1+\nu_a)(1-2\nu_a)}\varepsilon_\theta(x)+\frac{\nu_a E_a}{(1+\nu_a)(1-2\nu_a)}(\varepsilon_x(x)+\varepsilon_r(x)), \tag{16c}$$

where E_a, ν_a are the Young modulus and the Poisson's ratio for the adhesive material.

It is interesting to note that if we consider identical material and cross-section areas for the two tubes ($\nu=\nu_1=\nu_2$, $EA=E_1A_1=E_2A_2$) we obtain $\varepsilon_\vartheta=-\nu\varepsilon_x$ with $\varepsilon_x=N/(2EA)$. This physically means that the strain in the adhesive layer along the x-direction is simply imposed by the elongation of the tubes supposed loaded with a constant force equal to its mean value. In these hypothesis the normal stresses (16) assume the form $\sigma_{x,r,\theta}(x)\approx B+D(f(x)-1/2)$ with B, D constants (Fig. 4). Being $R/h\gg 1$ ($B/D\approx 0$) the stress peaks, at the end of the adhesive layer, become $\sigma_{\substack{x,\vartheta\\ \max}}\approx\mp\nu_a\nu/((1+\nu_a)(1-2\nu_a))E_aRN/(EhA)$, $\sigma_{\substack{r\\ \max}}\approx(1-\nu_a)/\nu_a\sigma_{\substack{x,\vartheta\\ \max}}$, i.e., proportional to $E_aRN/(EhA)$.

4 Stress Concentration Factor

The main problem related to the stress peaks is connected to the predominant tangential stress field (14), that in fact cannot be deleted, being equivalent to the applied axial load. On the other hand, the normal stress field (16) has a mean value equal to zero with maximum stresses independent of the function f, that must satisfy the boundary conditions (6). For these reasons we focus our attention on the tangential stress field (14).

Considering Eq. (14) it is possible to define a stress concentration factor which indicates the extent to which maximum shear stress departs from the mean. The higher stress peak appears at the end of the stiffer tube ($x=\bar{c}$):

$$\tau_{\substack{rx\\ \max}}=\tau_{rx}(x=\bar{c})=\frac{N\alpha}{2\pi R}(-C_1e^{\alpha\bar{c}}+C_2e^{-\alpha\bar{c}}),$$

$$\bar{c}=\begin{cases}-c & 0<\beta<\dfrac{1}{2}\\ c & \dfrac{1}{2}\leqslant\beta<1\end{cases}. \tag{17}$$

The mean value of the stress is

$$\tau_{\substack{rx\\ \text{mean}}}=\frac{1}{2c}\int_{-c}^{+c}\tau_{rx}(x)dx=\frac{N}{4\pi Rc}. \tag{18}$$

Consequently, the stress concentration factor is given by

$$\lambda=\frac{\tau_{\substack{rx\\ \max}}}{\tau_{\substack{rx\\ \text{mean}}}}=2\alpha c(-C_1e^{\alpha\bar{c}}+C_2e^{-\alpha\bar{c}}). \tag{19}$$

Of importance is the gain parameter λ^*, i.e., the index of the gain in maximum stress leveling which can be obtained by increasing the bond length. In this context, it should be noted that as the bond length tends to infinity, the maximum stress tends asymptotically to a minimum nonzero value:

$$\tau_{\substack{rx\\ \max\\ \min}}=\lim_{c\to\infty}\tau_{\substack{rx\\ \max}}=\frac{N\alpha\beta}{2\pi R}. \tag{20}$$

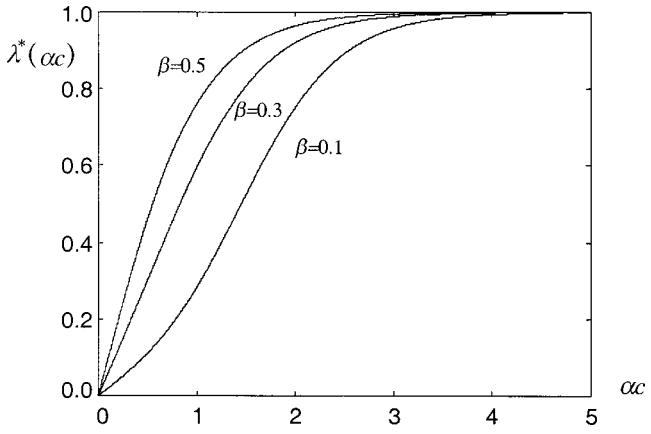

Fig. 5 Gain parameter $\lambda^*(\alpha c)$

For example, if we consider identical material and cross-section areas for the two tubes, we have $\tau_{\substack{rx\\ \max\\ \min}} = \sqrt{G_a/(EARh)}N/(2\sqrt{\pi})$. The gain parameter can thus be defined as

$$\lambda^*(\alpha c) = \frac{\tau_{\substack{rx\\ \max\\ \min}}}{\tau_{\substack{rx\\ \max}}} = \frac{\beta}{(-C_1 e^{\alpha c} + C_2 e^{-\alpha c})}, \tag{21}$$

and must be as close to unity as it is compatible with the need for a compact joint. Under this assumption the stress concentration factor, prudently overestimated, is detailed as follows:

$$\lambda \cong 2\alpha\beta c \quad \text{for } \lambda^* \cong 1. \tag{22}$$

Figure 5 shows that gain parameter λ^* presents little variation after a certain value of the nondimensional parameter αc ($\sim$3); consequently, further increases in bond length are pointless for the axial strength. Furthermore β must be equal to 1/2 (same stiffness EA for the two tubes) to have a symmetric stress field. Under these assumptions the stress concentration factor appears to be close to 3, an often-used value in elastic problems. This value for the stress concentration factor is very common for the stress peaks in the adhesive layer of tubular and nontubular bonded joints, [10,11].

5 Optimization for Uniform Axial Strength (UAS)

In order to obtain a unit value for the stress concentration factor given by Eq. (19) it is possible to modify the joint profile. This is achieved by chamfering the edges, which are in any case not involved in the tube stress flow induced by the axial load.

The procedure used is a reversal of that employed for a joint of known geometry: rather than starting from the geometry in order to determine the stress field, the procedure starts with the stress field and determines the geometry capable of ensuring it.

In order to make the predominant stress component (1) constant, it must be independent of the x-coordinate. In other words, as shown by relation (14), the load must be linear along the joint x-axis:

$$f(x) = \left(\frac{1}{2} - \frac{x}{2c}\right). \tag{23}$$

Inserting Eq. (23) in Eq. (10) yields the following relation, which defines the geometry of a uniform axial strength (UAS) adhesive bonded joint:

$$\frac{E_2A_2(x)}{E_1A_1(x)} = \frac{c+x}{c-x}, \tag{24}$$

that represents the equation governing the UAS profile. From Eq. (24) we can seen that the cross-section area of the two optimized tubes must go to zero at the end of the adhesive layer.

Though the number of possible shapes which satisfy the relations indicated above is infinite, the following additional condition must be considered in order to obtain the solution entailing tubes with symmetric stiffness section by section:

$$E_1A_1(x) = E_2A_2(-x), \tag{25}$$

that permits to have an identical stiffness EA for the two tubes out of the bonded area. As a consequence, we obtain the following optimized UAS profiles:

$$E_1A_1(x) = \frac{c-x}{2c}EA, \quad E_2A_2(x) = \frac{c+x}{2c}EA. \tag{26}$$

For example, if we consider identical material and cross-section areas for the two tubes, supposed with thin thickness s_i, we have $s_1(x) \approx (c-x)/(2c)\cdot s$, $s_2(x) \approx (c+x)/(2c)\cdot s$ with $s_1 + s_2 = s$. For this particular case the optimization is corresponding to a perfectly linear tapering of the adherends.

In this context, it should be noted that as the bond length tends to infinity, the stress (equal to the mean value expressed by Eq. (18)) tends asymptotically to a minimum zero value. This is a very important behavior of the UAS joint because theoretically, differently from a nontapered joint, the adhesive can withstand every axial load simply modifying its length surface. This upper bound of force, increasing the adhesive length, for nontapered adherends is (supposing identical material and cross-section areas for the two tubes, and the collapse when $\tau_{\substack{rx\\ \max}} = \tau_f$) $N_f(c \to \infty) = \sqrt{4\pi RhEA/G_a}\,\tau_f$, and is infinity for the optimized joint.

The optimization permits to have a constant tangential stress and also a large reduction in the normal stresses. Putting Eq. (23) into Eq. (14) we obtain the tangential stress in the UAS joint:

$$\tau_{\substack{rx\\ \text{UAS}}} = \frac{N}{4\pi Rc}. \tag{27}$$

Putting Eqs. (23) and (26) into Eqs. (15), supposing to simplify the equations $\nu = \nu_1 = \nu_2$, we obtain the dilations in the UAS joint: $\varepsilon_r = 0$, $\varepsilon_\theta = -\nu N/(EA)$, $\varepsilon_x = N/A$. Putting them into Eqs. (16) we obtain the normal stresses in the UAS joint that appear constants along the x-axis:

$$\sigma_x = \frac{1-\nu_a-\nu\nu_a}{(1+\nu_a)(1-2\nu_a)}\frac{E_aN}{EA}, \tag{28a}$$

$$\sigma_r = \frac{\nu_a-\nu\nu_a}{(1+\nu_a)(1-2\nu_a)}\frac{E_aN}{EA}, \tag{28b}$$

$$\sigma_\vartheta = \frac{\nu_a-\nu+\nu\nu_a}{(1+\nu_a)(1-2\nu_a)}\frac{E_aN}{EA}, \tag{28c}$$

i.e., proportional to $E_aN/(EA)$. For nonoptimized joint the maximum normal stresses are of the order of $E_aRN/(EhA)$, so that the optimization has provided a theoretical reduction by a factor R/h (1,2, or 3 order of magnitude).

However, it is important to note that adhesive bonded joints could be susceptible to brittle collapse. In order to take advantage of the UAS joint geometry it is essential that appropriate technological measures be introduced to ensure that joint collapse cannot involve mechanical fracture phenomena.

6 Energy Balance During Crack Propagation

By virtue of the energy balance, the following relationship between the variation in the total potential energy dW and the fracture energy $\mathcal{G}$ dS must hold:

$$\mathcal{G}\,\mathrm{d}S + \mathrm{d}W = 0, \tag{29}$$

where dS represents the incremental fracture surface area.

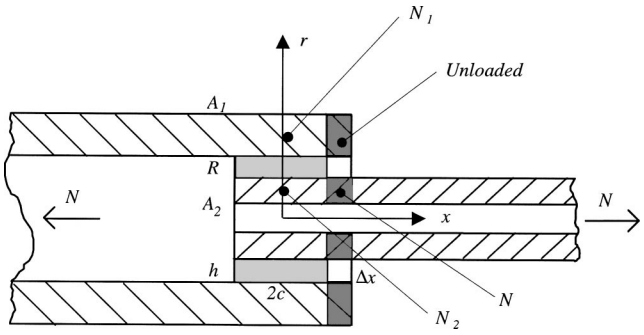

Fig. 6 Adhesive debonding for tubular adhesive joint subjected to axial load

Considering an imposed axial load, the variation in the total potential energy is equal to

$$dW = dL - N du = d\left(\frac{1}{2} N u\right) - N du = -dL, \tag{30}$$

where dL denotes the variation in the elastic strain energy (evaluated by virtue of Clapeyron's Theorem), N is the external load, and u its dual displacement. The strain energy release rate can be rewritten as

$$\mathcal{G} = -\frac{dW}{dS} = \frac{dL}{dS}. \tag{31}$$

Brittle crack propagation really occurs when $\mathcal{G}$ reaches its critical value $\mathcal{G}_a$, characteristic for the adhesive:

$$\mathcal{G} = \frac{dL}{dS} = \mathcal{G}_a. \tag{32}$$

The propagation will be stable, metastable, or unstable depending on the sign of the second-order derivative of the total potential energy:

$$-\frac{d^2W}{dS^2} = \frac{d\mathcal{G}}{dS} = \frac{d^2L}{dS^2} \begin{cases} <0, & \text{stable} \\ =0, & \text{metastable} \\ >0, & \text{unstable} \end{cases} \tag{33}$$

7 Joint Elastic Strain Energy

To solve the problem of the crack propagation it is necessary to evaluate the elastic strain energy of the joint as a function of the crack length (in the overlap zone, during crack propagation it being constant out of the overlap). The energy L absorbed by the joint is the sum of three quantities, i.e., the elastic strain energy absorbed by the two tubular bars (pedex 1,2) and by the adhesive (pedex 3):

$$L = L_1 + L_2 + L_3. \tag{34}$$

As previously shown, the predominant shearing stress field in the adhesive (equivalent to the applied normal thrust) has its maximum positive value at the end of the stiffer tubular bar (here indicated by 1). The initial separation at the interface between the two adherends is supposed to take place in this point: the debond is a crown-crack of length Δx (Fig. 6). The elastic strain energy of the cracked joint along the overlap can be calculated, noting how the portions of the joint are loaded. Fixing the origin of the x-axis at the middle of the ligament of length $2c$-Δx of the adhesive (see Fig. 6), we have

$$L_1 = \int_{-c+\Delta x/2}^{c-\Delta x/2} \frac{N_1^2(x)}{2E_1A_1(x)}\,dx, \tag{35}$$

$$L_2 = \int_{-c+\Delta x/2}^{c-\Delta x/2} \frac{N_2^2(x)}{2E_2A_2(x)}\,dx + \int_{c-\Delta x/2}^{c+\Delta x/2} \frac{N^2}{2E_2A_2(x)}\,dx, \tag{36}$$

that are integrals of known functions—see Eqs. (5), (11).

The elastic strain energy absorbed by the adhesive of the cracked joint is equal to

$$L_3 = \int_{-c+\Delta x/2}^{c-\Delta x/2} \left\{ \frac{1}{2E_a}[\sigma_x^2(x) + \sigma_r^2(x) + \sigma_\vartheta^2(x)] - \frac{\nu_a}{E_a}[\sigma_x(x)\sigma_r(x) + \sigma_x(x)\sigma_\vartheta(x) + \sigma_\vartheta(x)\sigma_r(x)] + \frac{\tau_{rx}^2(x)}{2G_a} \right\} 2\pi R h\,dx, \tag{37}$$

that is an integral of known functions—see Eqs. (16). Applying Eq. (31), we can obtain the strain energy release rate $\mathcal{G}$, where $dS = 2\pi R\,d(\Delta x)$. Equation (32) represents the condition of brittle crack propagation. Equation (33) shows whether the fracture propagation is stable, metastable or unstable.

8 Strength and Stability Under Crack Propagation

If we suppose that the height h of the adhesive layer tends to zero (and as a consequence $L_3 \to 0$), the functions f_i will assume the physical meaning of coefficients of distribution:

$$f_i(x) = \frac{E_iA_i(x)}{E_1A_1(x) + E_2A_2(x)}; \quad -c < x < c. \tag{38}$$

In the case of constant high profiles, functions (38) are constant along $x (x \neq \pm c)$ and, putting them into Eqs. (35) and (36), we obtain the joint elastic strain energy ($L = L_1 + L_2$). From Eq. (32) we obtain the strength of the joint, i.e., the critical value for the axial load corresponding to the crack propagation:

$$N_C = \sqrt{4\pi R \mathcal{G}_a \frac{E_2A_2}{E_1A_1}(E_1A_1 + E_2A_2)}, \quad \frac{E_2A_2}{E_1A_1} < 1. \tag{39}$$

Applying Eq. (33), or observing that N_C is not a function of the crack length, we can deduce that the propagation will be metastable:

$$\frac{dN_C}{d(\Delta x)} = 0 \Rightarrow \text{metastable}. \tag{40}$$

Equation (39) represents an extension of the critical condition presented, and experimentally verified for the particular case of $E_1A_1 \to \infty$, [19]. In addition, the presented approach to study the strength of the joint against brittle crack propagation has already been experimentally validated for the case of nontubular joints, [20].

For uniform axial strength joint, connecting tubular bars with identical stiffness EA, the adherends must be tapered with the profiles of Eq. (26). These profiles are the best from a tensional point of view. In this case, Eqs. (35) and (36) must be rewritten taking into account the symmetrical propagation by the length $\Delta x/2$ of the crack at the end of the two tubular bars:

$$L_1 = \int_{-c+\Delta x/2}^{c-\Delta x/2} \frac{N_1^2(x)}{2E_1A_1(x)}\,dx + \int_{-c}^{-c+\Delta x/2} \frac{N^2}{2E_1A_1(x)}\,dx = L_2 = \int_{-c+\Delta x/2}^{c-\Delta x/2} \frac{N_2^2(x)}{2E_2A_2(x)}\,dx + \int_{c-\Delta x/2}^{c} \frac{N^2}{2E_2A_2(x)}\,dx. \tag{41}$$

Equation (39) becomes

$$N_C = \sqrt{4\pi R \mathcal{G}_a \frac{4c - \Delta x}{\Delta x} EA} \quad \text{(UAS joint)}. \tag{42}$$

Applying Eq. (33), or observing that for UAS joint an increase in the crack length causes a reduction in the load of brittle failure, we can deduce that the propagation will be unstable:

$$\frac{dN_C}{d(\Delta x)}<0 \Rightarrow \text{unstable (UAS joint)}. \tag{43}$$

Summarizing, for conventional joints the load of brittle failure is independent of the crack length and the propagation will be metastable, when the load reaches its critical value of Eq. (39). On the other hand, for UAS joints an increasing of the crack length causes a reduction in the load of brittle failure and the propagation will be unstable, when the load reaches its critical value of Eq. (42). In this case, for vanishing pre-existing defects in the adhesive layer ($\Delta x \to 0$), the critical value of Eq. (42) tends to infinity. This simply means that the joint will collapse due to a different mechanism (we will discuss this transition in the following section). As a consequence, the UAS joint, good bonded, is stronger than the conventional one against brittle collapse. In addition, it is interesting to note that tubular joints are ''shape-resistant'' (the strength is different from zero also without adhesive) with respect to shear and flexure but not with respect to thrust and torque. For these reasons, axial load and torsional moment are more critical than shear and flexure for this kind of joints. Furthermore, for UAS and UTS, [11], (i.e., uniform torsional strength) the optimizations coincide for thin tubes. This means that optimized thin tubes present a global optimization design.

9 Ductile-Brittle Transition

The effective critical load is provided by the lower between the load of brittle crack propagation (39) or (42) and the load of ductile collapse. If we assume that the latter is achieved when the maximum shearing stress in the ligament of the adhesive layer equals its ultimate stress τ_u, and that c is not too short ($\alpha c \geqslant 3$, in the hypothesis of Eq. (22)), we obtain the following ultimate load of ductile collapse for conventional and optimized joint:

$$N_U = \sqrt{\frac{2\pi R h}{G_a}\frac{E_2A_2}{E_1A_1}(E_1A_1+E_2A_2)}\,\tau_u, \quad \frac{E_2A_2}{E_1A_1}<1, \tag{44}$$

$$N_U = 2\pi R(2c-\Delta x)\tau_u \quad \text{(UAS joint)}. \tag{45}$$

Comparing the critical values of the loads of brittle—see Eqs. (39), (42)—and ductile collapse—see Eqs. (44), (45)—the brittleness number s of the joint may be defined, [13,14,20]:

$$\frac{N_C}{N_U} = \mu s; \quad \begin{cases} \mu = \sqrt{2}; & s = \dfrac{\sqrt{\mathcal{G}_a G_a}}{\sqrt{h}\,\tau_u}; \\ \mu = \sqrt{\dfrac{1}{\pi}\dfrac{4c/\Delta x - 1}{(2c/\Delta x - 1)^2}\dfrac{A}{\Delta x^2}}; & s = \dfrac{\sqrt{\mathcal{G}_a E}}{\sqrt{R}\,\tau_u} \quad \text{(UAS joint)}. \end{cases} \tag{46}$$

Considering different sizes of self-similar joints the introduced parameter μ is a constant. The brittleness number s shows how the brittle collapse tends to occur with a low fracture energy, a low elastic modulus, a high ultimate stress and/or a large structural size. It is not the individual values of the parameters that are responsible for the nature of the collapse mechanism, but rather only their function s. By Eqs. (39), (42), and (45), (46), we can predict the strength of conventional and UAS joints.

10 Crack Detection by Axial Natural Frequencies

The crack length Δx is a priori unknown. In this section we present a theoretical approach to evaluate this parameter as a function of the axial natural frequencies of the cracked joint. It can be used as a detection method to predict crack severity. The axial natural frequencies can be experimentally obtained from conventional nondestructive tests of axial vibration.

The equation of motion of the overlap in a dynamic regime, [21], can be written introducing the inertia of the tubular bar in the joint equilibrium Eq. (9):

$$\frac{\partial N_1(x,t)}{\partial x} - \rho_1(x)A_1(x)\frac{\partial^2 u_1(x,t)}{\partial t^2} + K^*(x)(u_2(x,t)-u_1(x,t)) = 0, \quad 1 \leftrightarrow 2, \tag{47}$$

where ρ_i is the mass density (and u_i the displacement) of the ith tube. Furthermore,

$$N_1(x,t) = E_1(x)A_1(x)\frac{\partial u_1(x,t)}{\partial x}, \quad 1 \leftrightarrow 2. \tag{48}$$

Putting Eq. (48) into Eq. (47), we obtain the dynamic equations

$$\frac{\partial}{\partial x}\left(E_1(x)A_1(x)\frac{\partial u_1(x,t)}{\partial x}\right) - \rho_1(x)A_1(x)\frac{\partial^2 u_1(x,t)}{\partial t^2} + K^*(x)(u_2(x,t)-u_1(x,t)) = 0, \quad 1 \leftrightarrow 2. \tag{49}$$

To obtain a closed-form solution, we have to consider tubular bars of identical materials and cross-section areas. In these hypothesis, Eq. (49) becomes

$$EA\frac{\partial^2 u_1(x,t)}{\partial^2 x} - \rho A\frac{\partial^2 u_1(x,t)}{\partial t^2} + K^*(x)(u_2(x,t)-u_1(x,t)) = 0, \quad 1 \leftrightarrow 2. \tag{50}$$

If we consider $\rho \to 0$ in Eq. (50), it reduces to the static equilibrium of the joint. On the other hand, if $K^* \to 0$ we obtain the conventional dynamic equilibrium equation for a tubular bar.

In order to derive the equations, and due to the different field equations ruling the axial vibrations in and outside the bonding region, it is necessary to divide both tubular bars in different sections. As a consequence, Sections 1 and 2 of the first tubular bar define the region out of (the corresponding dynamic equilibrium is imposed by Eq. (50) in which we put $K^*=0$) and inside (Eq. (50) with $K^* \neq 0$) the bonding. For the second tubular bar, Sections 3 and 4 define the region in (Eq. (50) with $K^* \neq 0$ and $1 \to 2$) and outside (Eq. (50) with $K^*=0$ and $1 \to 2$) the bonding, respectively. Section 5 is the cracked region for the first tubular bar (Eq. (50) with $K^*=0$). See Fig. 7.

For all these cases, Eq. (50) can be written in the following unified manner (by sum and subtraction of the two equations for which $K^* \neq 0$):

$$\frac{\partial^2 \varphi(x,t)}{\partial t^2} - \xi\frac{\partial^2 \varphi(x,t)}{\partial x^2} + \zeta\varphi(x,t) = 0, \tag{51}$$

where $\xi = E/\rho$ and

$$\varphi(x,t) = u_1(x,t) \quad \zeta = 0, \tag{52}$$

$$\varphi(x,t) = u_2(x,t) - u_3(x,t) \quad \zeta = \frac{2K^*}{\rho A}, \tag{53}$$

$$\varphi(x,t) = u_2(x,t) + u_3(x,t) \quad \zeta = 0, \tag{54}$$

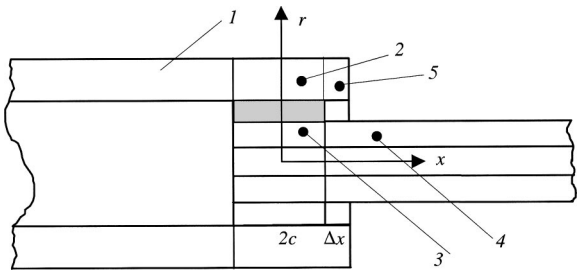

Fig. 7 Regions 1–5 of the cracked tubular bonded joint governed by different axial dynamic equations. Coupled regions (by the adhesive) are 2–3.

$$\varphi(x,t)=u_4(x,t) \quad \zeta=0, \tag{55}$$

$$\varphi(x,t)=u_5(x,t) \quad \zeta=0, \tag{56}$$

where, to simplify the notation, we have indicated with u_i the displacement in the mentioned ith section.

By applying the separation of variables, the solution of Eq. (50) can be written as superposition of solutions of the form

$$\varphi(x,t)=\psi(x)\phi(t), \tag{57}$$

so that Eq. (50) becomes

$$\frac{1}{\phi(t)}\frac{\mathrm{d}^2\phi(t)}{\mathrm{d}t^2}=\frac{\xi}{\psi(x)}\frac{\mathrm{d}^2\psi(x)}{\mathrm{d}x^2}-\zeta=-\omega^2, \tag{58}$$

where the natural circular frequency ω is a constant. We have, therefore,

$$\phi(t)=\sin(\omega t+\vartheta), \tag{59}$$

$$\psi(x)=A\sin(\lambda x)+B\cos(\lambda x), \tag{60}$$

with

$$\lambda^2=\frac{\omega^2-\zeta}{\xi}. \tag{61}$$

By introducing Eqs. (59) and (60) into Eqs. (52)–(56), it is possible to determine the corresponding expression for $u_i(x,t)=u_i(x)\sin(\omega t+\vartheta)$:

$$u_1(x)=A_1\sin(\lambda x)+B_1\cos(\lambda x), \tag{62a}$$

$$u_2(x)=\frac{1}{2}[A_2\sin(\overline{\lambda}x)+B_2\cos(\overline{\lambda}x)+A_3\sin(\lambda x)+B_3\cos(\lambda x)], \tag{62b}$$

$$u_3(x)=\frac{1}{2}[-A_2\sin(\overline{\lambda}x)-B_2\cos(\overline{\lambda}x)+A_3\sin(\lambda x)+B_3\cos(\lambda x)], \tag{62c}$$

$$u_4(x)=A_4\sin(\lambda x)+B_4\cos(\lambda x), \tag{62d}$$

$$u_5(x)=A_5\sin(\lambda x)+B_5\cos(\lambda x), \tag{62e}$$

where

$$\lambda^2=\frac{\rho}{E}\omega^2, \quad \overline{\lambda}^2=\frac{\rho}{E}\omega^2-\frac{2K^*}{EA}. \tag{63}$$

If $\omega\to 0$, we obtain the static solution. If $2L$ is the overall length of the joint, the boundary conditions at the left and right end are ($'\equiv \mathrm{d}/\mathrm{d}x$):

$$u_1(-L)=u_1'(-L)=0, \tag{64}$$

for free ends, or

$$u_4(L)=u_4'(L)=0, \tag{65}$$

for clamped ends.

The remaining boundary conditions impose the continuity of the axial displacement and of its derivative, i.e., of the axial load (Fig. 7):

$$u_1(-(c-\Delta x/2))=u_2(-(c-\Delta x/2)), \tag{66a}$$

$$u_1'(-(c-\Delta x/2))=u_2'(-(c-\Delta x/2)), \tag{66b}$$

$$u_2'(c-\Delta x/2)=u_5'(c-\Delta x/2), \tag{66c}$$

$$u_2(c-\Delta x/2)=u_5(c-\Delta x/2), \tag{66d}$$

$$u_5'(c+\Delta x/2)=0, \tag{66e}$$

$$u_3'(-(c-\Delta x/2))=0, \tag{66f}$$

$$u_3(c-\Delta x/2)=u_4(c-\Delta x/2), \tag{66g}$$

$$u_3'(c-\Delta x/2)=u_4'(c-\Delta x/2). \tag{66h}$$

Equations (64) and (65) and (66e) can be rewritten taking into account Eqs. (62) as

$$A_1=-\tan(\lambda L+n_l\pi/2)B_1=C_1B_1, \tag{67a}$$

$$A_4=\tan(\lambda L-n_r\pi/2)B_4=C_4B_4, \tag{67b}$$

$$A_5=\tan(\lambda(c+\Delta x/2))B_5=C_5B_5, \tag{67c}$$

where n_l and n_r refer to the left and right end, respectively, and they are equal to 0 or 1 if the corresponding end is whether free or clamped. The entire system of algebraic boundary conditions can be rewritten taking into account Eqs. (62) as

$$[M(\omega_n(\Delta x))]\{X\}=\{0\}, \tag{68}$$

where

$$[M]=\begin{bmatrix} \overline{S} & S & 2(C+C_1S) & -\overline{C} & -C & 0 & 0 \\ -\overline{C}^* & -C & 2(S-C_1C) & -\overline{S}^* & -S & 0 & 0 \\ \overline{C}^* & C & 0 & -\overline{S}^* & -S & 0 & 2(S-CC_5) \\ -\overline{S} & S & 0 & -\overline{C} & C & -2(C+C_4S) & 0 \\ -\overline{C}^* & C & 0 & \overline{S}^* & -S & 2(S-C_4C) & 0 \\ -\overline{C}^* & C & 0 & -\overline{S}^* & S & 0 & 0 \\ \overline{S} & S & 0 & \overline{C} & C & 0 & -2(C+SC_5) \end{bmatrix}, \tag{69}$$

and

$$\overline{S}=\sin(\overline{\lambda}(c-\Delta x/2)),\quad \overline{S}^{*}=\lambda^{*}\sin(\overline{\lambda}(c-\Delta x/2)),$$
$$\overline{C}=\cos(\overline{\lambda}(c-\Delta x/2)),\quad \overline{C}^{*}=\lambda^{*}\cos(\overline{\lambda}(c-\Delta x/2)),\quad (70)$$
$$S=\sin(\lambda(c-\Delta x/2)),\quad C=\cos(\lambda(c-\Delta x/2)),$$

with $\lambda^{*}=\overline{\lambda}/\lambda$. Furthermore,

$$\{X\}^{T}=[A_2A_3B_1B_2B_3B_4B_5]. \quad (71)$$

In order to obtain a nonzero solution, it is necessary to find the eingvalues $\omega_n(\Delta x)$ so that

$$\det[M(\omega_n(\Delta x))]=0. \quad (72)$$

The eigenvalues $\omega_n(\Delta x)$ are the axial natural circular frequencies of the bonded joint with a crack of length Δx, with corresponding eigenvectors (or modeshapes) given by $\{X_n(\Delta x)\}$:

$$[M(\omega_n(\Delta x))]\{X_n(\Delta x)\}=\{0\}. \quad (73)$$

The numerical solution of Eq. (72) provides, in a very simple way, the crack length as a function of the natural frequencies, considering a joint of given material and geometry. Some numerical examples of solution of determinantal equation like Eq. (73)—for undamaged joint under torsion—can be found in [21]. If $\Delta x\rightarrow 0$, we obtain the dynamic behavior of the undamaged bonded joint.

From the displacement (62) we can obtain the predominant stress field in the vibrating adhesive:

$$\tau_{rx}(x,t)=\frac{K^{*}\Delta u(x,t)}{2\pi R}. \quad (74)$$

The remaining components of the stress field can be obtained substituting the static load with the dynamic one of Eq. (48) in the static adhesive stresses of Eqs. (16).

Conclusions

The optimal profile for uniform axial strength, even if purely theoretical, could give useful guidelines to designers of tubular bonded joints under axial load. This optimal shape would permit both reduced weight and increased strength. The constant shearing stress field in the bond would enable the adhesive to withstand large axial loads by simply modifying the adhesive length. Also the normal stresses are strongly reduced by optimization. On the other hand, the developed fracture energy criterion permits to predict the critical load due to brittle crack propagation and the stability of the process. UAS and UTS profiles (uniform axial and uniform torsional strength), optimizing the joint from a stress point of view, coincide for thin tubes. In addition, the proposed approach shows that the optimized profile implies also a decrease in the brittleness of the joint. This is a relevant result for a global optimization design.

The axial natural frequencies of the cracked joint have been evaluated by determining the roots of a determinantal equation. The latter has been written by deriving the equation of motion for the cracked joint in axial vibrations and by imposing the related boundary conditions. This approach permits to evaluate the crack length as a function of the (experimental) axial natural frequencies.

References

[1] Beevers, A., 1999, "Durability Testing and Life Prediction of Adhesive Joints," Int. J. Mat. Prod. Tech., **14**, pp. 373–384.

[2] Goland, M., and Reissner, E., 1944, "The Stresses in Cemented Joints," ASME J. Appl. Mech., **11**, pp. 17–27.

[3] Lubkin, J. L., and Reissner, E., 1956, "Stress Distribution and Design Data for Adhesive Lap Joints Between Circular Tubes," Trans. ASME, **78**, pp. 1213–1221.

[4] Adams, R. D., and Peppiatt, N. A., 1977, "Stress Analysis of Adhesive Bonded Tubular Lap Joints," J. Adhes., **9**, pp. 1–18.

[5] Renton, W. J., and Vinson, J. R., 1977, "Analysis of Adhesively Bonded Joints Between Panels of Composite Materials," ASME J. Appl. Mech., **44**, pp. 101–106.

[6] Delale, F., and Erdogan, F., 1981, "Viscoelastic Analysis of Adhesively Bonded Joints," ASME J. Appl. Mech., **48**, pp. 331–338.

[7] Chen, D., and Cheng, S., 1983, "An Analysis of Adhesive-Bonded Single-Lap Joints," ASME J. Appl. Mech., **50**, pp. 109–115.

[8] Pugno, N., 1999, "Optimizing a Non-Tubular Adhesive Bonded Joint for Uniform Torsional Strength," Int. J. of Materials and Product Technology, **14**, pp. 476–487.

[9] Pugno, N., 2001, "Closed Form Solution for a Non-Tubular Bonded Joint With Tapered Adherends Under Torsion," Int. J. Mech. Control, **2**, pp. 19–27.

[10] Pugno, N., and Surace, G., 2000, "Non-Tubular Bonded Joint Under Torsion: Theory and Numerical Validation," Struct. Eng. Mech., **10**, pp. 125–138.

[11] Pugno, N., and Surace, G., 2001, "Tubular Bonded Joint Under Torsion: Analysis and Optimization for Uniform Torsional Strength," J. Strain Anal. Eng. Des., **1**, pp. 17–24.

[12] Griffith, A. A., 1921, "The Phenomena of Rupture and Flow in Solids," Philos. Trans. R. Soc. London, Ser. A, **221**, pp. 163–198.

[13] Carpinteri, A., 1981, "Static and Energetic Fracture Parameters for Rocks and Concretes," Materials and Structures, **14**, pp. 151–162.

[14] Carpinteri, A., 1989, "Cusp Catastrophe Interpretation of Fracture Instability," J. Mech. Phys. Solids, **37**, pp. 567–582.

[15] Carpinteri, A., 1989, "Decrease of Apparent Tensile and Bending Strength With Specimen Size: Two Different Explanations Based on Fracture Mechanics," Int. J. Solids Struct., **25**, pp. 407–429.

[16] Carpinteri, A., 1989, "Size Effects on Strength, Toughness and Ductility," J. Eng. Mech. Div., **115**, pp. 1375–1392.

[17] Carpinteri, A., 1989, "Softening and Snap-Back Instability in Choesive Solids," Int. J. Numer. Methods Eng., **28**, pp. 1521–1537.

[18] Carpinteri, A., 1997, *Structural Mechanics—A Unified Approach*, E&FN Spon.

[19] Gent, A. N., and Yeoh, O. H., 1982, "Failure Loads for Model Adhesive Joints Subjected to Tension, Compression or Torsion," J. Mater. Sci., **17**, pp. 1713–1722.

[20] Pugno, N., and Carpinteri, A., 2002, "Strength, Stability and Size Effects in the Brittle Behavior of Bonded Joints Under Torsion: Theory and Experimental Assessment," Fatigue Fract. Eng. Mater. Struct., **25**, pp. 55–62.

[21] Pugno, N., and Ruotolo, R., 2002, "Evaluation of Torsional Natural Frequencies for Non-Tubular Bonded Joints," Structural Engineering and Mechanics, **13**, pp. 91–101.

[22] Withney, J. M., and Pagano, N. J., 1970, "Shear Deformation in Heterogeneous Anisotropic Plates," ASME J. Appl. Mech., **37**, pp. 1031–1036.

[23] Newill, J. F., and Vinson, J. R., 1993, "Some High Strain Rate Effects on Composite Materials," *Proceedings of the 9th International Conference on Composite Materials*, Part 5, July 12–16, pp. 269–277.

[24] Bigwood, D. A., and Crocombe, A. D., 1990, "Non-Linear Adhesive Bonded Joints Design Analysis," Int. J. Adhes. Adhes., **10**, pp. 31–41.

[25] Gibson, R. F., 1994, *Principles of Composite Material Mechanics*, McGraw-Hill, New York.

[26] Moloney, A. C., Kausch, H. H., and Stieger, H. R., 1984, "The Use of the Double Torsion Test Geometry to Study the Fracture of Adhesive Joints," J. Mater. Sci. Lett., **3**, pp. 776–778.

[27] Surace, G., and Brusa, E., 1995, "A Parametric Study of Structural Adhesive Joints for Aerospace Applications," *Advanced Technology for Design and Fabrication of Composite Materials and Structures*, G. C. Sih, A Carpinteri, and G. Surace, eds., Kluwer, Dordrecht, The Netherlands.

[28] Tsai, M. Y., and Morton, J., 1994, "Three-Dimensional Deformations in a Single-Lap Joints," J. Strain Anal., **29**, pp. 137–145.